LA-UR- 97-3027

CONF-970407--

Title: Simulations of Linear and Nonlinear Rayleigh-Taylor Instability Under High Atwood Numbers

Author(s): C. K. Choi, N. M. Hoffman, M.R. Clover
W. J. Powers

Submitted to: Proceeding of 1997 Laser Interactions & Related Plasma Phenomena (LIRPP)

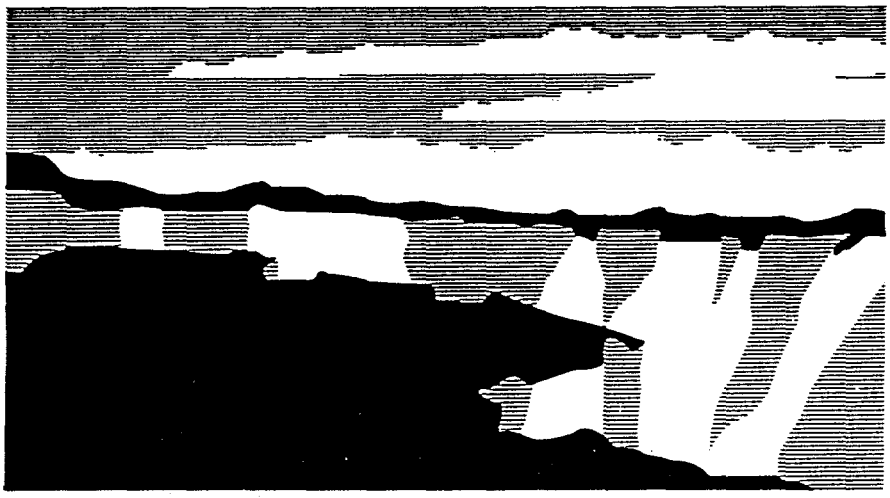

Los Alamos
NATIONAL LABORATORY

Form No. 836 R5
ST 2629 10/91

DISCLAIMER

Simulations of Linear and Nonlinear Rayleigh-Taylor Instability under High Atwood Numbers

C. K. Choi*, N. M. Hoffman, M. R. Clover, and W. J. Powers
*Purdue University, West. Lafayette, IN 47907
Los Alamos National Laboratory, Los Alamos, NM 87545

Abstract. Inertial confinement fusion (ICF) implosions, whether real or ideal, are subject to a variety of hydrodynamic instabilities that amplify small departures from spherical symmetry. Asymmetric implosions departing from spherical symmetry can lead to the breakup of the imploding shell or the creation of hydrodynamic turbulence. In an effort to understand the evolution of the asymmetries, perturbation "seeds" with both velocity and surface displacements have been introduced at the boundary of two different density media to model analytical Rayleigh-Taylor instability growth. Growth of perturbed amplitudes has been studied in linear and late-time nonlinear regimes. Simulated linear growth rates and nonlinear bubble velocities are in good agreement with theoretical values for Atwood numbers that are close to unity (relevant to ICF applications).

I INTRODUCTION

Hydrodynamic instabilities [1,2] and the Rayleigh-Taylor (RT) instability, in particular, impose an upper limit on the value of the shell in-flight aspect ratio (IFAR), which results in a minimum pressure or absorbed driver irradiance. The IFAR is defined as the ratio of the shell radius, R, as it implodes to its compressed thickness, ΔR. Asymmetric implosions departing from spherical symmetry can lead to the breakup of the imploding shell or the creation of hydrodynamic turbulence. Hence, the control of RT-induced mix of hot and cold fuel is crucial to the successful formation of the central hot spot for efficient thermonuclear burn with the proposed National Ignition Facility (NIF) targets [3].

The major objective of the current study is to understand the evolution of the asymmetries by following in time the perturbation "seeds" that are simulated by velocity and/or surface displacements introduced at the boundary of two different density media. As a first step towards validating numerical

simulations of ICF ablative RT instability growth, we look at our ability to model pure RT instabilities in incompressible fluids.

The simulated linear growth rates of the "seeded" perturbed amplitudes are studied first with separate velocity and surface displacements and then with combined velocity and surface displacements. The simulated growth rates are compared with the theoretical values of γ, where $\gamma = \sqrt{kgA}$ with k, g, and A being the wave number, gravitational acceleration, and the Atwood number, respectively. The Atwood number is defined as $A = \frac{(\rho_1 - \rho_2)}{(\rho_1 + \rho_2)}$, where ρ_1 and ρ_2 are mass densities in the two different media. Furthermore, the bubble velocities (v_b) that develop in the late-time nonlinear regime are also analyzed by comparison with the theoretical values of the bubble velocities, $v_b = \alpha\sqrt{\frac{2A}{(1+A)}g\lambda}$, where α is a coefficient balancing a bubble drag and buoyancy with $0.2 \leq \alpha \leq 0.3$ [4,5], and λ is the wavelength. In the present simulation, both the gravitational acceleration (g) and the wavelength (λ) are defined to be unity. Thus, the unit of distance is λ, the unit of time is $\sqrt{\lambda/g}$, and the unit of velocity is $\sqrt{g\lambda}$.

In an effort to simulate the RT instability that is pertinent to the actual inertial confinement fusion environment, high density ratios between the two different media, typically 1:10, are simulated, i.e., high Atwood numbers (A) approaching to unity.

The numerical simulations employ the 2-D Langragian hydrodynamics code LASNEX – with a new prescription for the "artificial" viscosity tensor, $\mathcal{Q}$. It was essential to use this more correct hydro method in validating the RT simulations, because a pure quadratic $\mathcal{Q}$ could not even run the problem, let alone get the correct growth rates. The $\mathcal{Q}$ used is:

$$\mathcal{Q} = (\frac{1}{2}\rho v \Delta x)(\nabla \cdot \vec{u}^{ltd})\hat{s}\hat{s},$$

where

$$\hat{s} = \frac{\Delta\vec{u}}{|\Delta\vec{u}|},$$

$$v = C_s + \frac{\Gamma + 1}{2}(\Delta u)^{<},$$

$$(\Delta u)^{<} = |\min(\nabla \cdot \vec{u}^{ltd}, 0)|,$$

$$(\nabla \cdot \vec{u})^{ltd} = (\nabla \cdot \vec{u}) \cdot [1 - \max(0, \min(\frac{R_L + R_R}{2}, 2R_L, 2R_R, 1))],$$

and

$$R_L = \frac{(\nabla \cdot \vec{u})_{z-1}}{(\nabla \cdot \vec{u})_z}\ ,\ R_R = \frac{(\nabla \cdot \vec{u})_{z+1}}{(\nabla \cdot \vec{u})_z}.$$

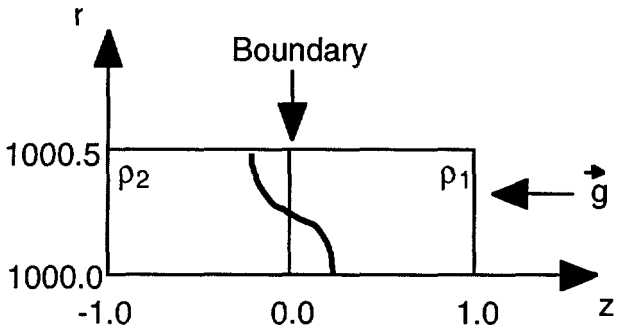

FIGURE 1. Initial problem set up with the velocity displacement introduced at the boundary.

Here the notations, u and v, indicate fluid velocity and Hugoniot velocity, respectively; C_s referes to the speed of sound ($C_s = \sqrt{\frac{\Gamma p}{\rho}}$), and Γ is the specific heat ratio ($\Gamma = \frac{C_p}{C_v} = \frac{5}{3}$). When the limiters ($2R_L$, $2R_R$) do not turn on, $(\nabla \cdot u)^{ltd}$ is a higher order (centered, therefore second order) approximation to the velocity jump in a zone. $z \pm 1$ refers to the zones to the top/bottom or left/right of the face in question. Effects of both high Atwood numbers and perturbation amplitude on RT instability will also be discussed.

II DESCRIPTION OF PROBLEM SET UP

The problem was set up in r-z planar geometry with two different density media in an incompressible fluid regime as illustrated in Fig. 1. The mesh was moved far from the symmetry axis ($r = 0$), in order to approximate x-y geometry in an r-z code. Density ratios varied from $\frac{1}{2}$ to $\frac{1}{11}$ to $\frac{1}{50}$, resulting in Atwood numbers $\frac{1}{3}$, $\frac{5}{6}$, and $\frac{49}{51}$. Perturbation displacement and velocity amplitudes of $\sim 10^{-4}$ were introduced along the half-wavelength interface boundary.

The number of zones per wavelength along the r-axis was varied from 20 to 100; i.e., 10 to 50 along the r-axis per half wavelength (l_z). The number of zones along the z-axis was also made variable, in order to investigate mass-matching as well as equi-spacing across the density jump.

In order to ensure incompressibility, high temperatures were introduced such that the sound speeds were $\gg 1$. This pressure gradient then exactly balanced the force of gravity (which acts in the negative-z direction) in the unperturbed case. All conduction was turned off.

Three types of problems were set up: an initial interface velocity (v_0) but no interface displacement, an initial interface displacement (z_0) but no interface velocities, and a combined set of both perturbations, where $z_0 = v_0/\gamma$. Furthermore, all nodal velocities (and/or displacements) in the mesh were set

proportional to an eigenmode ($\sim \exp(\pm kz)$) consistent with initial conditions at the interface.

III THE LINEAR RT INSTABILITY AND EFFECTS OF HIGH ATWOOD NUMBERS

Both square zones and mass-matched geometry were studied with various number of zones per wavelength for varying Atwood numbers. Velocity vs. time values were converted into linear growth rates [$\gamma = \frac{1}{t}\ln(\frac{v_z}{v_{z_0}})$] and the growth rates were analyzed as functions of number of zones and mesh sizes. In general, γ was obtained by a least-squares regression fit to a selected "straight" section of the data. The code that did the fits searched over all possible combinations of a delimited range of points to find the best solution (correlation coefficient closest to unity), which was used as the final result.

Solutions of the linear Rayleigh-Taylor problem are linear combinations of $\exp(-\gamma t)$ and $\exp(\gamma t)$, or equivalently, of $\cosh(\gamma t)$ and $\sinh(\gamma t)$. For initial velocity perturbations alone, the solution with the correct initial condition is $v(t) = v_0\cosh(\gamma t)$, $z(t) = \frac{v_0}{\gamma}\sinh(\gamma t)$ at the interface. For initial interface perturbations alone, the solution with the correct initial condition is $v(t) = \gamma z_0\sinh(\gamma t)$,$z(t) = z_0\cosh(\gamma t)$ at the interface. If both the interface and its velocity are perturbed consistently (with $v_0 = \gamma z_0$), the solution is $v(t) = v_0\exp(\gamma t)$, $z(t) = z_0\exp(\gamma t)$ at the interface. Solutions, $v(t)$, for these three cases are shown in Fig. 2. The calculated vs. theoretical growth rates are compared and plotted in Fig. 3 for Atwood number $\frac{1}{3}$ with square and mass-matched zones, as are growth rates for Atwood numbers $\frac{5}{6}$ and $\frac{49}{51}$.

It is apparent from Fig. 3 that square zones converge more quickly to the correct theoretical value, though at higher number of zones (or smaller mesh sizes) the linear growth rates with high Atwood number, $A = \frac{49}{51}$, encounter numerical noise. For $A = \frac{5}{6}$ and $A = \frac{1}{3}$, square mesh zones behave remarkably well, approaching the theoretical value quickly. We take this to indicate that with equal spacing, we are solving the equations accurately to order $(\Delta x)^2$; mass-matched zoning is only accurate to order Δx. For $A = \frac{49}{51}$, regardless of zoning method, there is a smallest zone size below which the simulations no longer appear to converge. We presume that roundoff errors begin to dominate the imposed perturbations at that point. (We are only plotting the interface velocity at the lower boundary, not the amplitude of the lowest Fourier component of the velocity profile along the whole interface. Thus when roundoff seeds higher modes, they will grow faster and dominate sooner.) More efforts were exerted on the sensitivity to perturbation amplitudes for both linear and late-time nonlinear analyses of RT instabilities, which will be described in the next section.

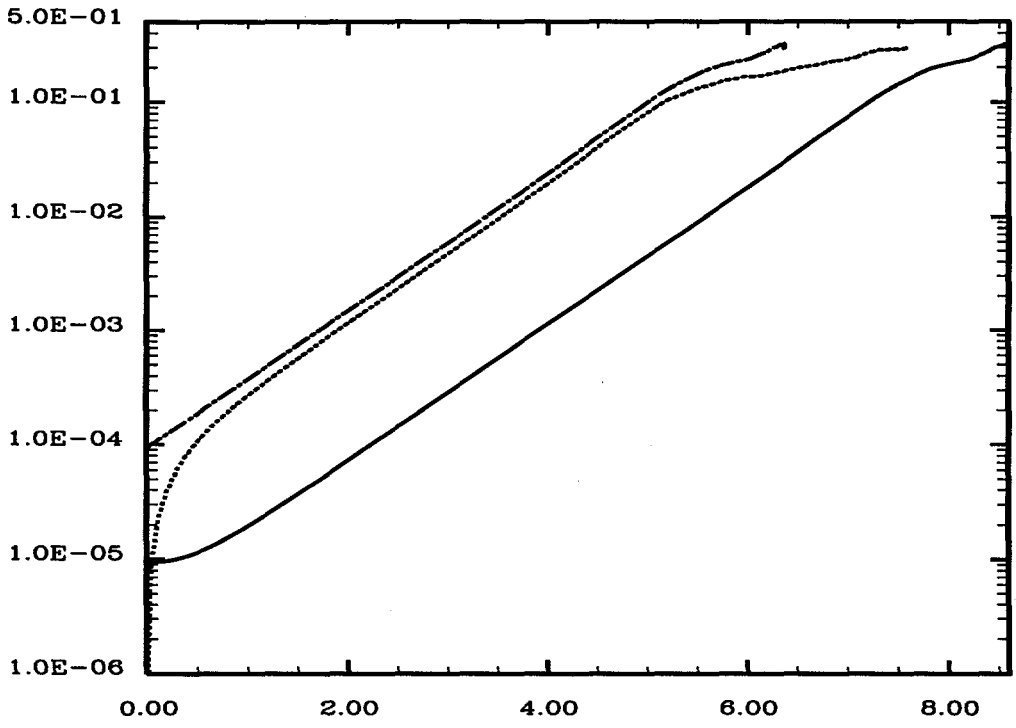

FIGURE 2. Interface velocity versus time for Atwood number $\frac{1}{3}$ for velocity perturbation amplitudes(solid), surface perturbation amplitudes (dotted) and combined velocity and surface perturbation amplitudes(dot-dashed).

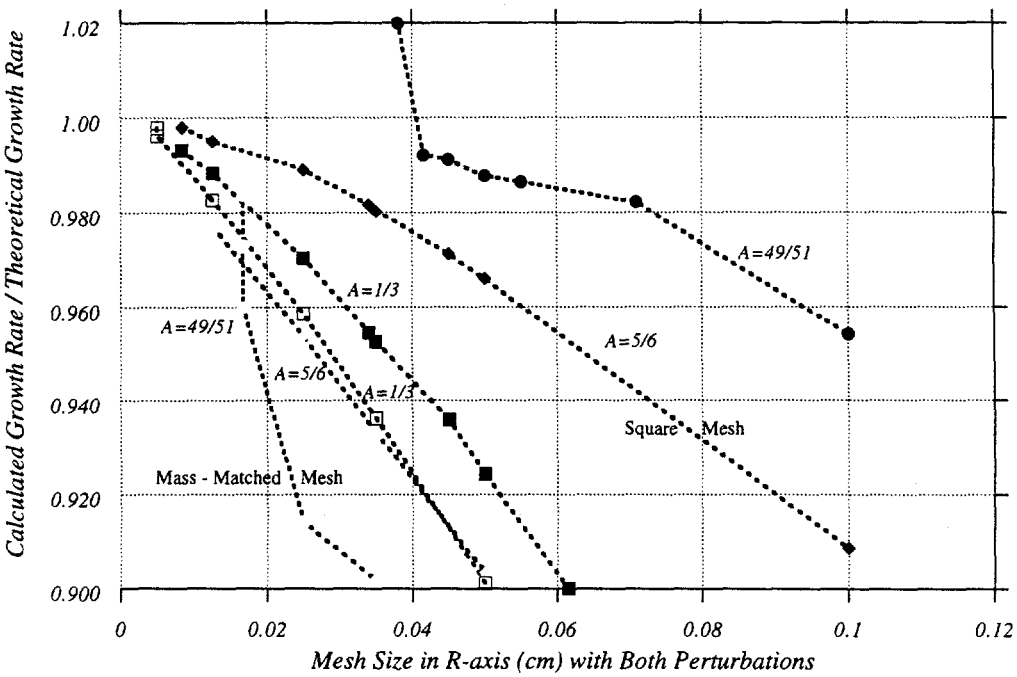

FIGURE 3. Ratio of calculated to theoretical growth rates vs. mesh size for various Atwood numbers

IV EFFECTS OF PERTURBATIONS ON LINEAR AND BUBBLE GROWTH RATES

A Linear Growth Rates

In order to quantify the dependence of linear growth rates on perturbation amplitudes, the perturbation amplitude (v_0) has been varied from 10^{-4} to 10^{-3} for the low Atwood number $A = \frac{1}{3}$. The linear growth rates have been computed for half-wavelength radial zonings $l_z = 28, 22$, and 8 as well as for $l_z = 10, 20$, and 40 that were studied earlier. As illustrated in Fig. 4, for a small number of zones like $l_z = 8$, the growth rates between 10^{-3} and 10^{-4} are remarkably different; as mesh sizes get smaller (or large number of zones like $l_z = 40$), the difference in growth rates for both initial perturbation amplitudes converge to a common value predicted by theory. It would be interesting but not necessary at this point to show that the same trend may hold with yet smaller perturbation amplitude, $v_0 = 10^{-5}$ (if round-off errors do not dominate). The convergence to a common value of theoretical growth rates indicates that the true value of the linear growth rates does not depend on the magnitude of perturbation amplitudes, as one would expect from linear perturbation theory.

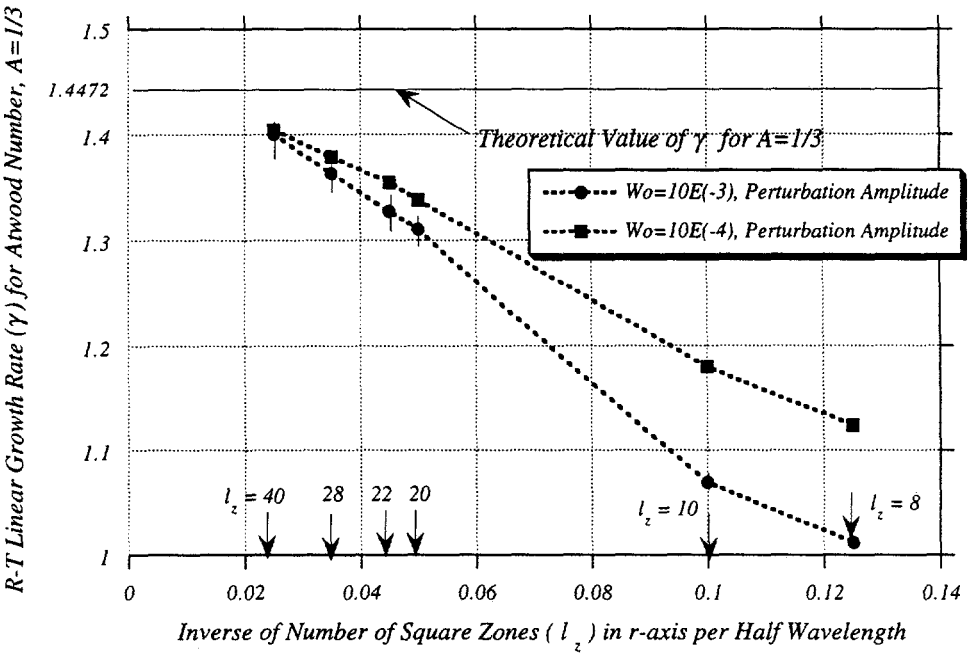

FIGURE 4. Linear growth rates vs. mesh size for different perturbation amplitudes.

TABLE 1. Linear growth rates (γ) and bubble velocities (v_b). Note: $\alpha = 0.25$ ($0.2 \leq \alpha \leq 0.3$) was used to evaluate v_b (theory).

Density		Atwood	γ(theory),	γ	v_b(theory),	v_b
ρ_1	ρ_2	Number	$\sqrt{Akg}$	(calculated)	$\alpha\sqrt{\frac{2A}{1+A}g\lambda}$	(calculated)
1	5/7	1/6	1.0233	1.0233 (100%)	0.1336	0.130 (97.3%)
1	1/2	1/3	1.4472	1.4375 (99.3%)	0.1767	0.170 (96.2%)
1	1/11	5/6	2.2882	2.2839 (99.8%)	0.2383	0.220 (92.3%)
1	1/50	49/51	2.4569	2.4378 (99.2%)	0.2474	0.225 (90.9%)

B Nonlinear Bubble Growth Rates

It is interesting to note though that unlike the linear growth rates in Fig. 3 there was no functional dependence of the bubble velocities on mesh sizes. Late-time nonlinear bubble velocities are difficult to analyze as a function of mesh size due to the fact that there appears to be no clear bubble saturation value; nevertheless, the ranges where bubble velocities are most likely to appear were well indicated as summarized in Table 1.

Bubble velocities for Atwood numbers other than $\frac{1}{3}$ have also been analyzed and the values have been tabulated in Table 1 which also includes the calculated linear growth rates (γ) for Atwood numbers $\frac{1}{6}$, $\frac{1}{3}$, $\frac{5}{6}$, and $\frac{49}{51}$ in good agreement with the theoretical values as shown in Table 1.

V SUMMARY AND CONCLUSIONS

The major objective of this work was to validate numerical simulations of Raleigh-Taylor instability growth by comparison with theoretical values, as a first step in understanding ablative Rayleigh-Taylor in ICF implosions. In particular, the main effort was to develop a simulation tool for hydrodynamic instability analysis for planar geometry with two different density media and with high Atwood numbers (e.g., $A \geq \frac{5}{6}$). The inherently compressible 2-D Lagrangian LASNEX was utilized to simulate incompressible fluids with high speeds of sound in a low density medium.

Consistent with physical intuition for incompressible fluids, square zones provided faster convergence than mass-matched rectangular mesh geometries. However, extremely fine mesh resolution led to undesirable numerical noise and mode mixing (round-off error growth) which are to be further explored with, for example, an automatic rezoner. It should be noted that higher order and limited artificial viscosities were essential in improving the overall simulation capabilities.

Different perturbation amplitudes (v_0) with 10^{-3} and 10^{-4} affected time evolution of bubble and spike velocities but did not alter physical results of linear growth rates as illustrated in Fig. 4.

As illustrated in Fig. 3 and Fig. 4 and as summarized in Table 1, it is apparent that linear RT growth rates (γ) and late-time nonlinear bubble velocities (v_b) can be simulated, and good agreement with the theoretical values can be achieved. In conclusion, the method of the present LASNEX simulations provide a tool for hydrodynamics instability analysis for ICF relevant high Atwood number cases.

REFERENCES

1. Chandrasekhar, S., *Hydrodynamic and Hydromagnetic Stability*, Oxford University Press, London (1961).
2. Hoffman, N. M., "Hydrodynamic Instabilities in Inertial Confinement Fusion," *Laser Plasma Interactions 5:Inertial Continement Fusion*, Hooper, M. B., ed., Institute of Physics Publishing, Bristol (1995), pp. 105-137.
3. Lindl, J., "Development of the indirect-drive approach to inertial confinement fusion and the target physics basis for ignition and gain," *Phys. Plasma*, 2(11), Nov.1995, 3933-4024.
4. D. Ofer, D. Shvarts, Z. Zinamon, and S.A. Orszag, "Mode Coupling in Nonlinear Rayleigh-Taylor instability, " *Phys. Fluids*, *B4* (1992) 3549.
5. Clover, M. R., Powers, W. J., and Choi, C.K., "Modeling of Bubble and Spike Velocities for a Rayleigh-Taylor Instability," in *Proceedings of the Fifth International Workshop on compressible Turbulent Mixing*: University of New York at Stony Brook, New York, USA, 18 -21 July, 1995, Young, R., Glimm, J., and Boston, B., eds., World Scientific, River Edge, NJ (1996), pp. 314-320.